INTERNATIONAL JOURNAL FOR NUMERICAL METHODS IN FLUIDS, VOL. 19, 395–413 (1994)

COMPUTATION OF FREE SURFACE WAVES AROUND AN ARBITRARY BODY BY A NAVIER–STOKES SOLVER USING THE PSUEDOCOMPRESSIBILITY TECHNIQUE

H. LIU

Kawachi Millibioflight Project, Research Development Corporation of Japan (JRDC), Park Building 3F, 4-7-6 Komaba, Meguro, Tokyo 153, Japan

AND

M. IKEHATA

Department of Naval Architecture and Ocean Engineering, Yokohama National University, 156 Tokiwadai, Hodogaya, Yokohama 240, Japan

SUMMARY

A Navier–Stokes equation solver is developed for computing free surface wave and viscous flow around an arbitrary body, in which a free surface model is introduced into the pseudocompressibility solution. The governing equations are classified in a vectorial form, with primitive variables, and a block diagonal system is generated by the discretization of an implicit factorization method. A moving grid system fitted to both the free surface and body surface is generated by an effective cubic spline fitting technique. Two zero-equation turbulence models, namely the Cebeci–Smith model and the Baldwin–Lomax model, are used for turbulent calculations. Numerical simulations are carried out for the free surface viscous flows generated by a submerged hydrofoil and a ship model. Computed results are in reasonable agreement with measurements.

KEY WORDS Euler implicit scheme Pseudocompressibility Moving grid system Free surface fitting Baldwin–Lomax turbulence model

1. INTRODUCTION

The flow around a ship is characterized by the presence of a free surface and viscosity. Until now the complicated interaction between wave and viscous flow and the uncertainty of the free surface configuration have made the solution of this problem very difficult. Accurate numerical prediction of waves generated by a ship is, however, very important from a practical standpoint, because the wave-making resistance has a rather sensitive property depending on factors such as hull form, the Froude number and so forth.

Previously many efforts have been made in the simulation of flow past a ship with a free surface by resolving the NS equations. In all cases the basic algorithm closely follows the MAC method, i.e.[1] solving a Euler equation with the SOR iterative method to obtain the pressure field and then correcting the velocity field using the momentum equations. The free surface configuration is evaluated by simultaneously moving the marker particles distributed previously on the free surface. Because the original MAC method used a spatially fixed Cartesian

CCC 0271–2091/94/170395–19

Received 17 December 1992
Revised 17 March 1994

co-ordinate system, which is not particularly well suited for the free surface flow around a ship-like body with a complicated geometry because of the use of a staggered mesh, many quasi-MAC methods[2,3] were subsequently developed based on the boundary-fitted curvilinear co-ordinate system proposed by Thompson *et al.*,[4] in which difficulties of interpolation near the free surface boundary are removed. Also, to increase the numerical stability, a fourth-order artificial numerical dissipation term is generally added to the convection terms for the high-Reynolds-number calculation, which, however, may result in the unexpected damping of waves. In addition, the explicit scheme for the momentum equations restricts the accuracy of the wave calculation and produces a small Courant number which needs a sufficiently small time increment when fine grids are used in order to achieve convergence.

The main objective of the present work is to develop another NS solver which introduces a free surface model into Chorin's artificial compressibility solution,[5] a standard technique for performing steady state incompressible flow calculations. Since one replaces the incompressibility condition by a time evolution equation for the pressure, intermediate results therefore become unphysical, but the equation of continuity will be satisfied in the steady state because the time derivative with respect to pressure then vanishes. With the pseudocompressibility technique the governing equations can be classified in a vectorial form and a block diagonal system is generated by the discretization of an implicit approximate factorization method,[6] which is very convenient for high-speed processing using vectorized computers such as a supercomputer.

A moving grid system is employed to provide a fit for both the free surface and body surface in order to satisfy boundary conditions easily, thus requiring regridding at each time step. To avoid consuming lengthy computer time in grid generation, a simple but effective grid generation method is developed which employs a cubic spline fitting technique. The basic idea is to consider each grid line as a two-dimensional or three-dimensional bending beam with both ends fixed. According to solid mechanics knowledge, with appropriate boundary conditions for the two ends and some loading on it, the bending beam will retain its orthogonality near both ends approximately with a certain form. In this respect, factors to assess grids, such as orthogonality, smoothing and clustering, are not difficult to satisfy. With this method a grid system fitted to both the deforming free surface and body surface can be obtained with less computer time, approximately 1% of the time being taken at one time step. To avoid the intersection of grid lines, Chan's rule[7] is used near the free surface and body surface; but how to control the grid line in an expected form, especially near complicated surfaces, remains a task to be solved in the future.

In order to make the algorithm similar to those for velocity and pressure, the free surface configuration is governed by the equation of the kinematic condition and is discretized in the same way as with the implicit scheme. Investigation of the non-linear free surface conditions for velocity and pressure shows that the stress condition on the free surface seems to make no significant difference in comparison with a zero-extrapolation approach for the high-Reynolds-number calculation. The Cebeci–Smith turbulence model is used for the two-dimensional turbulence calculation and the Baldwin–Lomax model for the three-dimensional simulation. The interaction between turbulence and free surface flow is not taken into consideration.

The present method embodies two computational codes for the simulations of free surface wave and viscous flow behind a hydrofoil and past a ship model. Validation analysis shows that both codes are able to estimate the free surface viscous flows reasonably well.

2. COMPUTATIONAL SCHEME

2.1. *Governing equations*

With the pseudocompressibility technique the non-dimensionalized governing equations in a Cartesian co-ordinate system become, if written in a vectorial form,

$$\mathbf{q}_t + \mathbf{E}\mathbf{q}_x + \mathbf{F}\mathbf{q}_y + \mathbf{G}\mathbf{q}_z = \mathbf{C}_R(\mathbf{q}_{xx} + \mathbf{q}_{yy} + \mathbf{q}_{zz}) + \mathbf{H}, \tag{1}$$

where

$$\mathbf{q} = \begin{bmatrix} u \\ v \\ w \\ p \end{bmatrix}, \qquad \mathbf{E} = \begin{bmatrix} u - 2v_x & -v_y & -v_z & 1 \\ 0 & u - v_x & 0 & 0 \\ 0 & 0 & u - v_x & 0 \\ \beta & 0 & 0 & 0 \end{bmatrix},$$

$$\mathbf{F} = \begin{bmatrix} v - v_y & 0 & 0 & 0 \\ -v_x & v - 2v_y & -v_z & 1 \\ 0 & 0 & v - v_y & 0 \\ 0 & \beta & 0 & 0 \end{bmatrix}, \qquad \mathbf{G} = \begin{bmatrix} w - v_z & 0 & 0 & 0 \\ 0 & w - v_z & 0 & 0 \\ -v_x & -v_y & w - 2v_z & 1 \\ 0 & 0 & \beta & 0 \end{bmatrix},$$

$$C_R = \left(\frac{1}{Re} + \nu\right)\begin{bmatrix} 1 & 0 & 0 & 0 \\ 0 & 1 & 0 & 0 \\ 0 & 0 & 1 & 0 \\ 0 & 0 & 0 & 0 \end{bmatrix}, \qquad \mathbf{H} = \begin{bmatrix} \dot{V} \\ 0 \\ -1/Fn^2 \\ 0 \end{bmatrix}.$$

In the fourth component of the above equations a time derivative of pressure is artificially added to the equation of continuity, which makes the system hyperbolic and the application of the implicit factorization method possible. The term β in the equation is a positive constant. In the case of computing a steady state flow by iterating in the time domain, the pseudocompressibility introduces no error in the converged solution, when all the derivatives with respect to time vanish, including the added $\partial p/\partial t$ term. Use of a large value of β allows time accuracy but makes the system of equations stiff and generally results in poor convergence. The inertia term $\dot{\mathbf{V}}$ is added for the acceleration process and $\mathbf{V}$ is defined as the velocity of the upstream boundary. Additionally, the following relation, in which hydrostatic pressure is excluded, is utilized instead of pressure p in order to simplify the algorithm:

$$\phi = p + z/Fn^2.$$

By substituting the above formula into equation (1), $\mathbf{q}$ and $\mathbf{H}$ become

$$\mathbf{q} = [u, v, w, \phi]^T, \qquad \mathbf{H}^* = [\dot{V}, 0, 0, 0]^T.$$

2.2. *Grid generation and co-ordinate transformation*

In order to make the scheme flexible and able to deal with boundaries of complex geometry in a straightforward manner, the moving grid system fitted to both the free surface and body is used. Thus a timely regridding is needed since the free surface deforms with time. Generally it is quite common that the trial and error of grid generation consumes a large percentage of the total computer time in solving the flow around a complicated body. Therefore the development

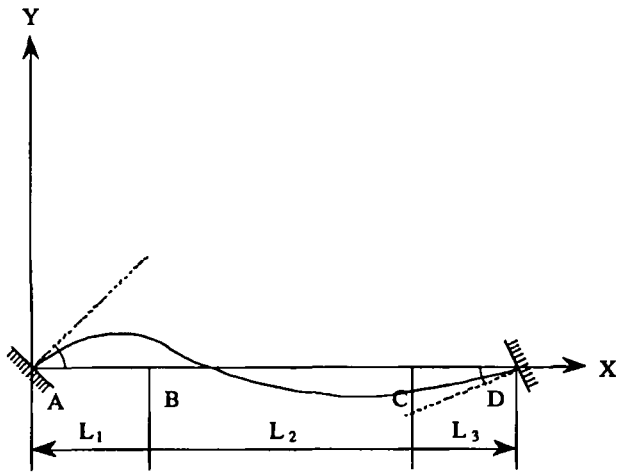

Figure 1. Grid line in local co-ordinate system

of a less time-consuming grid generation method is of great significance in the free surface calculation. In the present paper a grid generation method which employs a cubic spline fitting technique and is classified as an algebraic method is proposed. The idea of the method is mainly based on the beam-bending theory that each grid line can be considered as a two-dimensional or three-dimensional bending beam with both ends fixed. As is known, grid generation can be assessed by its orthogonality, smoothing, clustering and minimum grid spacing. From solid mechanics we know that a beam with both ends fixed under loading approximately retains its orthogonality near the two ends irrespective of the kind of load applied within its elastic limit. Thus a bending beam can be expressed as a polynomial and the grid lines demonstrate the properties of continuity and smoothing. Grid paints along a grid line are distributed with a power function which determines the grid division when the minimum grid spacing and grid number are given.

As illustrated in Figure 1, a grid line is defined to be composed of three curves, *curve*1, *curve* 2 and *curve*3, which are represented by third-order polynomial expressions in a local co-ordinate system (x, y) as

$$curve1: \quad y = a_0 + a_1 x + a_2 x^2 + a_3 x^3, \tag{2}$$

$$curve2: \quad y = b_0 + b_1 x + b_2 x^2 + b_3 x^3, \tag{3}$$

$$curve3: \quad y = c_0 + c_1 x + c_2 x^2 + c_3 x^3, \tag{4}$$

where x and y are co-ordinate values in the local co-ordinate system and a_i, b_i and c_i are coefficients to be determined under the smoothing continuity condition between curves and the orthogonality requirement at both ends. Furthermore, a three-dimensional grid line is considered as the linear combination of the two-dimensional grid lines. To avoid the intersection of grid lines near the free surface and body, Chan's rule is used.

The above boundary-fitted curvilinear co-ordinate system can be represented by the formulae

$$x = x(\xi, \eta, \zeta, t), \qquad y = y(\xi, \eta, \zeta, t), \qquad z = z(\xi, \eta, \zeta, t), \qquad \mathbf{q} = \mathbf{q}(x, y, z, t) = \mathbf{q}(\xi, \eta, \zeta, t)$$

Since the co-ordinate values of x, y and z change with time, the variables in physical space (u, v, w and ϕ) obey the formula

$$\frac{\partial}{\partial t_{(x,y,z)}} = \frac{\partial}{\partial t_{(\xi,\eta,\zeta)}} - \left(a\frac{\partial}{\partial \xi} + b\frac{\partial}{\partial \eta} + c\frac{\partial}{\partial \zeta}\right)x_t - \left(d\frac{\partial}{\partial \xi} + e\frac{\partial}{\partial \eta} + f\frac{\partial}{\partial \zeta}\right)y_t - \left(g\frac{\partial}{\partial \xi} + h\frac{\partial}{\partial \eta} + i\frac{\partial}{\partial \zeta}\right)z_t, \quad (5)$$

where

$$\begin{aligned} &a = \xi_x = J(y_\eta z_\zeta - y_\zeta z_\eta), \qquad b = \eta_x = J(y_\zeta z_\xi - y_\xi z_\zeta), \qquad c = \zeta_x = J(y_\xi z_\eta - y_\eta z_\xi),\\ &d = \xi_y = J(z_\eta x_\zeta - z_\zeta x_\eta), \qquad e = \eta_y = J(z_\zeta x_\xi - z_\xi x_\zeta), \qquad f = \zeta_y = J(z_\xi x_\eta - z_\eta x_\xi),\\ &g = \xi_z = J(x_\eta y_\zeta - x_\zeta y_\eta), \qquad h = \eta_z = J(x_\zeta y_\xi - x_\xi y_\zeta), \qquad i = \zeta_z = J(x_\xi y_\eta - x_\eta y_\xi),\\ &J = 1/S, \qquad S = x_\xi y_\eta z_\zeta + x_\eta y_\zeta z_\xi + x_\zeta y_\xi z_\eta - x_\xi y_\zeta z_\eta - x_\eta y_\xi z_\zeta - x_\zeta y_\eta z_\xi. \end{aligned} \quad (6)$$

Using the previously derived relations of variable transformation, the governing equations can be transformed into the curvilinear co-ordinate system as

$$\begin{aligned} \mathbf{q}_t + \mathbf{A}\mathbf{q}_\xi + \mathbf{B}\mathbf{q}_\eta + \mathbf{C}\mathbf{q}_\zeta = \mathbf{C}_R(&\hat{a}\mathbf{q}_{\xi\xi} + \hat{b}\mathbf{q}_{\eta\eta} + \hat{c}\mathbf{q}_{\zeta\zeta} + \hat{d}\mathbf{q}_{\xi\eta} + \hat{e}\mathbf{q}_{\eta\zeta}\\ &+ \hat{f}\mathbf{q}_{\zeta\xi} + \hat{g}\mathbf{q}_\xi + \hat{h}\mathbf{q}_\eta + \hat{i}\mathbf{q}_\zeta) + \mathbf{H}^* - \omega^\xi \frac{\partial^4 \mathbf{q}}{\partial \xi^4} - \omega^\eta \frac{\partial^4 \mathbf{q}}{\partial \eta^4} - \omega^\zeta \frac{\partial^4 \mathbf{q}}{\partial \zeta^4}, \end{aligned} \quad (7)$$

where

$$\mathbf{A} = a\mathbf{E}' + d\mathbf{F}' + g\mathbf{G}', \qquad \mathbf{B} = b\mathbf{E}' + e\mathbf{F}' + h\mathbf{G}', \qquad \mathbf{C} = c\mathbf{E}' + f\mathbf{F}' + i\mathbf{G}',$$

$$\mathbf{E}' = \mathbf{E} - x_t\mathbf{I}, \qquad \mathbf{F}' = \mathbf{F} - y_t\mathbf{I}, \qquad \mathbf{G}' = \mathbf{G} - z_t\mathbf{I}, \qquad \mathbf{I}\ a\ 4 \times 4\ \textit{unit matrix},$$

$$\hat{a} = a^2 + d^2 + g^2, \qquad \hat{b} = b^2 + e^2 + h^2, \qquad \hat{c} = c^2 + f^2 + i^2, \qquad \ldots.$$

Since central differencing is used in discretizing the convection terms, the fourth-order numerical dissipation terms are artificially added in order to damp numerical disturbances due to short wavelengths and enhance numerical stability.

2.3. *Approximate factorization*

A time derivative is replaced by a Padé time differencing

$$\frac{\partial}{\partial t} = \frac{1}{\Delta t}\frac{\Delta}{1 + \theta\Delta}, \quad (8)$$

where

$$\theta = \begin{cases} 0, & \text{Euler explicit,} \\ \frac{1}{2}, & \text{Crank–Nicolson,} \\ 1, & \text{Euler implicit.} \end{cases}$$

The parameter θ is set to unity in the present scheme, which makes the system a Euler implicit

scheme. By substituting equation (8) into equation (7) and approximate factorization, equation (7) can be decomposed into three components given by

ξ-sweep

$$\left\{\mathbf{I}+\theta\Delta t\left[\hat{\mathbf{A}}+\mathbf{A}\frac{\partial}{\partial\xi}-\mathbf{C}_{\mathrm{R}}\left(\hat{a}\frac{\partial^2}{\partial\xi^2}+\hat{g}\frac{\partial}{\partial\xi}\right)+\omega^{\xi}\frac{\partial^4}{\partial\xi^4}\right]^{(n)}\right\}\Delta\mathbf{q}^{*}$$
$$=-\Delta t[\mathbf{A}\mathbf{q}_{\xi}+\mathbf{B}\mathbf{q}_{\eta}+\mathbf{C}\mathbf{q}_{\zeta}-\mathbf{C}_{\mathrm{R}}(\hat{a}\mathbf{q}_{\xi\xi}+\hat{b}\mathbf{q}_{\eta\eta}+\hat{c}\mathbf{q}_{\zeta\zeta}+\hat{d}\mathbf{q}_{\xi\eta}+\hat{e}\mathbf{q}_{\eta\zeta}+\hat{f}\mathbf{q}_{\zeta\xi}$$
$$+\hat{g}\mathbf{q}_{\xi}+\hat{h}\mathbf{q}_{\eta}+\hat{i}\mathbf{q}_{\zeta})-\mathbf{H}^{*}]^{(n)}$$
$$-\Delta t\left(\omega^{\xi}\frac{\partial^4\mathbf{q}}{\partial\xi^4}+\omega^{\eta}\frac{\partial^4\mathbf{q}}{\partial\eta^4}+\omega^{\zeta}\frac{\partial^4\mathbf{q}}{\partial\zeta^4}\right)^{(n)}+\theta\Delta t\mathbf{C}_{\mathrm{R}}(\hat{d}\Delta\mathbf{q}_{\xi\eta}+\hat{e}\Delta\mathbf{q}_{\eta\zeta}+\hat{f}\Delta\mathbf{q}_{\zeta\xi})^{(n-1)}, \tag{9}$$

η-sweep

$$\left\{\mathbf{I}+\theta\Delta t\left[\hat{\mathbf{B}}+\mathbf{B}\frac{\partial}{\partial\eta}-\mathbf{C}_{\mathrm{R}}\left(\hat{b}\frac{\partial^2}{\partial\eta^2}+\hat{h}\frac{\partial}{\partial\eta}\right)+\omega^{\eta}\frac{\partial^4}{\partial\eta^4}\right]^{(n)}\right\}\Delta\mathbf{q}^{**}=\Delta\mathbf{q}^{*}, \tag{10}$$

ζ-sweep

$$\left\{\mathbf{I}+\theta\Delta t\left[\hat{\mathbf{C}}+\mathbf{C}\frac{\partial}{\partial\zeta}-\mathbf{C}_{\mathrm{R}}\left(\hat{c}\frac{\partial^2}{\partial\zeta^2}+\hat{i}\frac{\partial}{\partial\zeta}\right)+\omega^{\zeta}\frac{\partial^4}{\partial\zeta^4}\right]^{(n)}\right\}\Delta\mathbf{q}^{***}=\Delta\mathbf{q}^{**}; \tag{11}$$

updating

$$\mathbf{q}^{(n+1)}=\mathbf{q}^{(n)}+\Delta\mathbf{q}^{(n)}. \tag{12}$$

Here the convection terms are processed by the 'local linearization' as

$$\Delta(\mathbf{A}\mathbf{q}_{\xi})\doteq\Delta\mathbf{A}\mathbf{q}_{\xi}+\mathbf{A}\Delta\mathbf{q}_{\xi}$$
$$\doteq\hat{\mathbf{A}}\Delta\mathbf{q}_{\xi}, \tag{13}$$

where

$$\hat{\mathbf{A}}=\begin{bmatrix}au_{\xi} & du_{\xi} & gu_{\xi} & 0\\ av_{\xi} & dv_{\xi} & gv_{\xi} & 0\\ aw_{\xi} & dw_{\xi} & gw_{\xi} & 0\\ 0 & 0 & 0 & 0\end{bmatrix}. \tag{14}$$

Similarly $\Delta(\mathbf{B}\mathbf{q}_{\eta})$ and $\Delta(\mathbf{C}\mathbf{q}_{\zeta})$ are processed and $\hat{\mathbf{B}}$ and $\hat{\mathbf{C}}$ can also be obtained. $\Delta(\mathbf{q}^{*})$ and $\Delta(\mathbf{q}^{**})$ are intermediate variables, whereas $\Delta(\mathbf{q}^{***})$ is defined as the increment $\Delta\mathbf{q}$ at the nth time step. Spatial derivatives of ξ are approximated by five-point central differencing such that

$$\frac{\partial}{\partial\xi}=\tfrac{1}{12}(E^{-2}-8E^{-1}+8E^{+1}-E^{+2}),$$
$$\frac{\partial^2}{\partial\xi^2}=\tfrac{1}{12}(-E^{-2}+16E^{-1}-30E^{0}+16E^{+1}-E^{+2}), \tag{15}$$
$$\frac{\partial^4}{\partial\xi^4}=E^{-2}-4E^{-1}+6E^{0}-4E^{+1}+E^{+2},$$

and similarly for η and ζ.

Substituting equation (15) into equation (9) yields a set of linear, ordinary differencing equations given as

ξ-sweep

$$\mathbf{K}_i\Delta\mathbf{q}_{i-2} + \mathbf{L}_i\Delta\mathbf{q}_{i-1} + \mathbf{M}_i\Delta\mathbf{q}_i + \mathbf{N}_i\Delta\mathbf{q}_{i+1} + \mathbf{O}_i\Delta\mathbf{q}_{i+2} = \mathbf{f}_i, \tag{16}$$

where

$$\mathbf{K}_i = \frac{\theta\Delta t}{12}[\mathbf{A} + \mathbf{C}_R(\hat{a} - \hat{g}) + 12\omega^\xi\mathbf{I}], \qquad \mathbf{L}_i = \frac{\theta\Delta t}{12}[-8\mathbf{A} + 8\mathbf{C}_R(\hat{g} - 2\hat{a}) - 48\omega^\xi\mathbf{I}],$$

$$\mathbf{M}_i = \mathbf{I} + \frac{\theta\Delta t}{12}(12\mathbf{A} + 30\mathbf{C}_R\hat{a} + 72\omega^\xi\mathbf{I}), \qquad \mathbf{N}_i = \frac{\theta\Delta t}{12}[8\mathbf{A} - 8\mathbf{C}_R(\hat{g} + 2\hat{a}) - 48\omega^\xi\mathbf{I}], \tag{17}$$

$$\mathbf{O}_i = \frac{\theta\Delta t}{12}[-\mathbf{A} + \mathbf{C}_R(\hat{a} + \hat{g}) + 12\omega^\xi\mathbf{I}], \qquad \mathbf{f}_i = [\text{RHS of equation (9)}].$$

Similarly matrix coefficients can be obtained in the η- and ζ-sweeps.

At boundary locations three-point differencing is implemented to avoid the extrapolation of points outside the computational domain, thus minimizing numerical error there. Finally, with appropriate boundary conditions a block pentadiagonal linear system is formed which can be solved efficiently using a block pentadiagonal solver.

2.4. Boundary conditions

The boundary as illustrated in Figure 2 consists of an inflow, outflow, bottom, body surface, centre boundary, outer boundary and free surface. Boundary conditions used are as follows.

Inflow. Uniform velocity and zero pressure.

Outflow. Neumann (zero gradient) for velocity and pressure.

Centre boundary. Symmetry.

Body surface. No-slip for velocity and Neumann (zero gradient) for pressure.

Free surface. At the interface of air and water, considering the dynamic condition, i.e. the equilibrium of stresses on the free surface as illustrated in Figure 1, the stresses P_ξ, P_η and P_n are

$$P_\xi = \left(\frac{1}{Re} + \nu\right)e_i^\xi e_j^n(u_{i,j} + u_{j,i}), \qquad P_\eta = \left(\frac{1}{Re} + \nu\right)e_i^\eta e_j^n(u_{i,j} + u_{j,i}),$$

$$P_n = -P + 2\left(\frac{1}{Re} + \nu\right)e_i^n e_i^n u_{i,i},$$

where $e^\xi_{1,2,3}$, $e^\eta_{1,2,3}$ and $e^n_{1,2,3}$ are unit directional vectors. The stress components σ_{ij} are expressed in tensor form as

$$\sigma_{ij} = -P\delta_{ij} + \left(\frac{1}{Re} + \nu\right)(u_{i,j} + u_{j,i}). \tag{19}$$

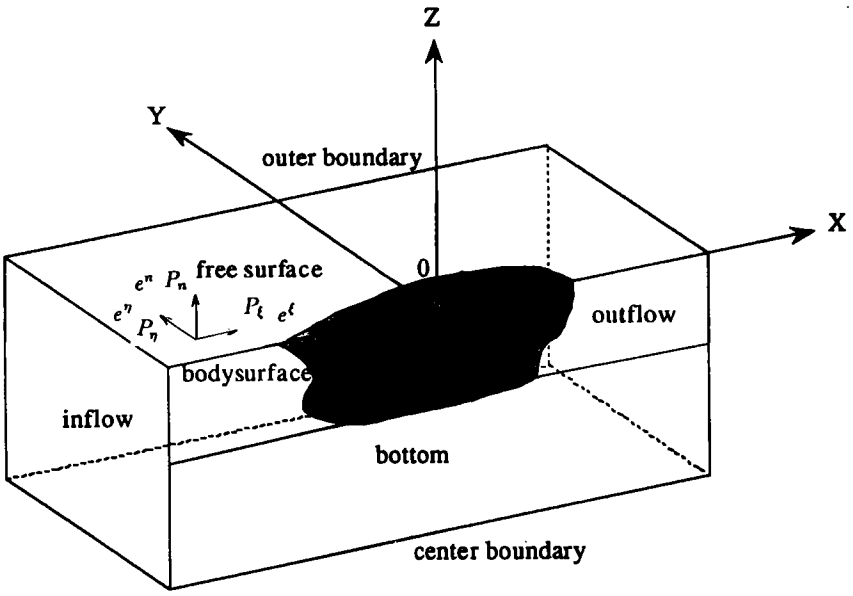

Figure 2. Co-ordinate system and boundaries

Notice that the third equation of (18) is mainly governed by the pressure term $-P$ in the case of high Re. Thus $P_n = -P$ represents a reasonable approximation. In addition, for the assumption of no wind stresses, the viscous terms multiplied by $1/Re + \nu$ can be set to zero such that

$$e_i^{\xi} e_j^{n} (u_{i,j} + u_{j,i}) = 0, \qquad e_i^{\eta} e_j^{n} (u_{i,j} + u_{j,i}) = 0, \qquad e_i^{n} e_i^{n} u_{i,i} = 0. \tag{20}$$

Therefore the boundary conditions for velocity and pressure on the free surface can be clarified as

$$\phi = h_{\text{free surface}}/Fn^2, \qquad u_{\zeta} = f_u, \qquad v_{\zeta} = f_v, \qquad w_{\zeta} = f_w, \tag{21}$$

where the formula for ϕ indicates that the pressure is equal to atmospheric pressure if surface tension is neglected, and f_u, f_v and f_w are functions of geometric quantities and velocity components on the free surface.

In the present study the surface tension and viscosity on the free surface are neglected because they negligibly affect the wave feature in the case of high Reynolds number, which will be discussed in Section 4. Thus a zero-extrapolation approach is used for velocity and the pressure is set to atmospheric pressure such that

$$u_{\zeta} = 0, \qquad v_{\zeta} = 0, \qquad w_{\zeta} = 0, \qquad \phi = h/Fn^2 \quad (p = p_a).$$

Outer boundary. Neumann (zero gradient) for velocity and pressure.

Bottom. Uniform velocity and zero pressure.

2.5. Turbulence model

For a free surface viscous flow problem a turbulence model which accounts for the free surface effect should be employed, because wave–turbulence interaction exists. Unfortunately, no such

turbulence model has been developed yet. In the present paper two zero-equation turbulence models, namely the Cebeci–Smith model[8] and the Baldwin–Lomax model, are employed for the two-dimensional and three-dimensional turbulence simulations respectively, in which the eddy viscosity is evaluated in different algebraic form in the inner and outer layers separately. The Baldwin–Lomax turbulence model is briefly described below.

On the solid wall

$$\nu = \begin{cases} \nu_{\text{inner}} = l^2|\omega|, \\ \nu_{\text{outer}} = \kappa C_{\text{cp}} F_{\text{kleb}} F_{\text{wake}}, \end{cases} \tag{22}$$

where

$$l = kn\left[1 - \exp\left(-\frac{n^+}{A^+}\right)\right], \qquad n^+ = nRe\sqrt{\tau_w}, \qquad k = 0{\cdot}4, \qquad A^+ = 26{\cdot}0.$$

The vorticity is expressed by ω and the shear stress on the solid wall by τ_w. The projection distance from some point on the η-line to the wall is represented by n. In addition,

$$F(n) = n|\omega|\left[1 - \exp\left(-\frac{n^+}{A^+}\right)\right], \qquad F_{\text{kleb}} = \left[1 + 5{\cdot}5\left(C_{\text{kleb}}\frac{n}{n_{\max}}\right)^6\right]^{-1},$$

$$F_{\text{wake}} = \min\left\{n_{\max}F_{\max}, C_{\text{wake}}U_{\text{diff}}^2\frac{n_{\max}}{F_{\max}}\right\},$$

$$\kappa = 0{\cdot}0168, \qquad C_{\text{cp}} = 1{\cdot}6, \qquad C_{\text{kleb}} = 0{\cdot}3, \qquad C_{\text{wake}} = 0{\cdot}25.$$

The maximum of $F(n)$ on the η-line is $F_{\max}$ and the n at that point is denoted by $n_{\max}$. The value of U_{diff} is calculated as the difference between the maximum and minimum of speed on the η-line. On the solid wall the smaller of ν_{inner} and ν_{outer} is chosen as ν. In the wake ν is taken to have the same form as ν_{outer} on the solid wall, but $F(n)$ has the simple form $n|\omega|$.

In the Baldwin–Lomax model, numerical calculation is convenient since the evaluation of the boundary layer is removed. The effect of transition to turbulence is neglected so that the flow is assumed to become turbulent everywhere in the boundary layer and in the wake. In the computational scheme the turbulent eddy viscosity ν is updated once every 20 time steps and is assumed to be time-independent during each 20 time steps so as to enhance the numerical stability and simplify the formulation.

3. NON-LINEAR CALCULATION OF FREE SURFACE ELEVATION

Generally waves are conventionally viewed as having a dynamic nature, but a towing tank test can give steady wave profiles and patterns around a ship model in a uniform flow. Thus, similarly to velocity and pressure, only the converged free surface configuration is physical. In order to get a similar system to that for velocity and pressure, the equation of the kinematic condition is chosen to compute the free surface elevation. The equation of the kinematic condition in computational space can be written as

$$\frac{\partial h}{\partial t} + U\frac{\partial h}{\partial \xi} + V\frac{\partial h}{\partial \eta} - W = 0. \tag{23}$$

Here the formula

$$\frac{\partial h}{\partial t_{(x,y)}} = \frac{\partial h}{\partial t_{(\xi,\eta)}} - \frac{\partial h}{\partial x} x_t - \frac{\partial h}{\partial y} y_t, \tag{24}$$

has been used, where

$$h = h(\xi, \eta, t), \qquad U = a(u - x_t) + d(v - y_t), \qquad V = b(u - x_t) + e(v - y_t), \qquad W = w.$$

Furthermore, since central differencing is also used for the convection-like terms $U\partial h/\partial\xi$ and $V\partial h/\partial\eta$, the fourth-order numerical dissipation terms are added to damp the short wavelengths such that

$$\frac{\partial h}{\partial t} + U\frac{\partial h}{\partial \xi} + V\frac{\partial h}{\partial \eta} - W + \omega^{h\xi}\frac{\partial^4 h}{\partial \xi^4} + \omega^{h\eta}\frac{\partial^4 h}{\partial \eta^4} = 0. \tag{25}$$

By discretizing with the same time and spatial differencing scheme as that of the governing equations for velocity and pressure in equation (7), the equation of the kinematic condition can be solved similarly with a pentadiagonal solver. The boundary conditions for the free surface elevation calculation are chosen to correspond to those for velocity and pressure.

4. COMPUTED RESULTS AND DISCUSSION

4.1. Two-dimensional problem

As a two-dimensional problem the numerical simulation of free surface waves and turbulent flow around a submerged hydrofoil (NACA0012 wing section), with an angle of attack of 5° at a Reynolds number $Re = 1{\cdot}0 \times 10^6$ and a Froude number $Fn = 0{\cdot}567$ at a submergence depth $d = 1{\cdot}29$, is carried out. An H-type grid topology as shown in Figure 3 (at $T = 16{\cdot}1$), with a region of $x(-3{\cdot}0, 4{\cdot}0)$, $y(-2{\cdot}79, 0{\cdot}0)$ and grids of 110×72, is used in order to treat the free surface boundary easily. In this case a cut boundary instead of a symmetrical boundary exists in front of and behind the body during the co-ordinate transformation, where a periodical condition is used. In the η-direction the grids are clustered to the solid wall with a minimum

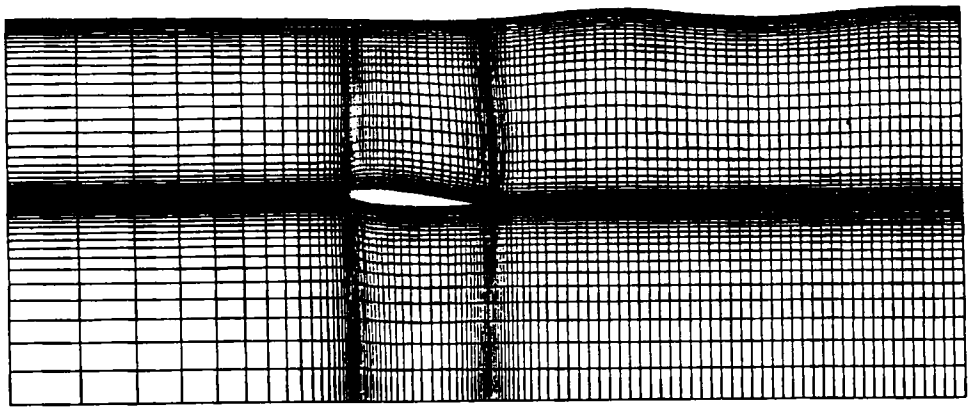

Figure 3. Grid system around NACA0012 wing section

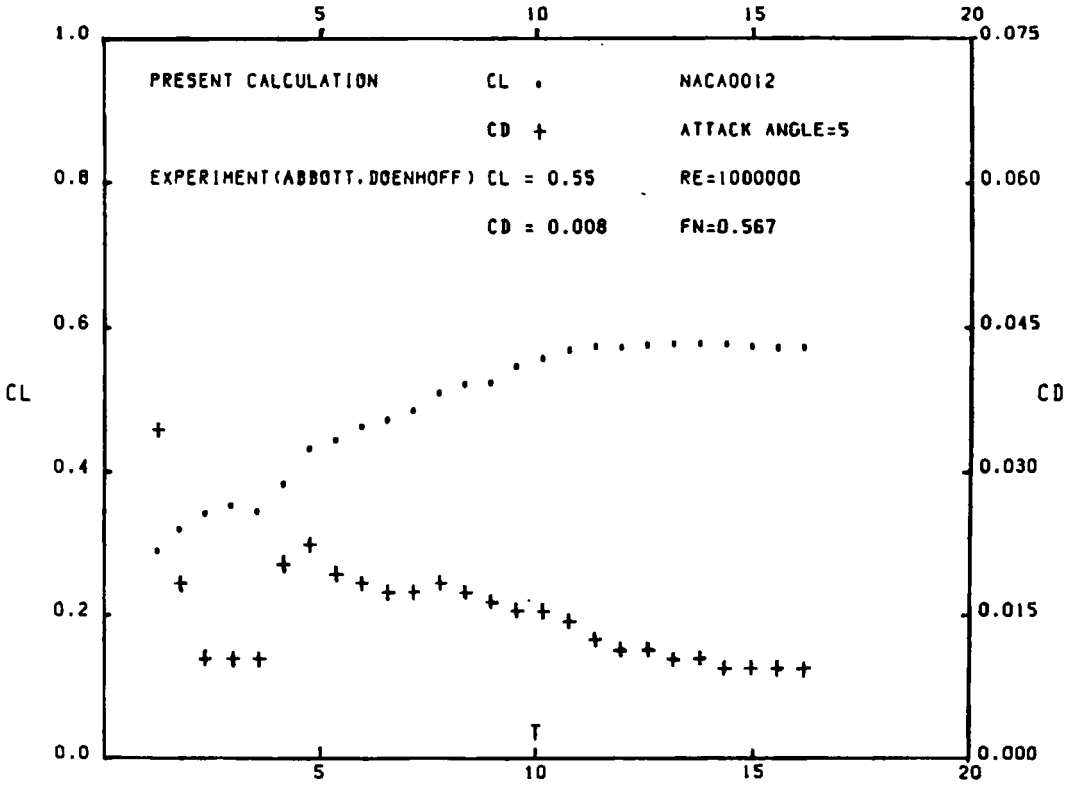

Figure 4. Lift and drag coefficients versus time (2D)

grid spacing of 0·001 adjacent to the wall, and to the free surface with a minimum grid spacing of 0·001. In the ξ-direction the grids are distributed densely near the leading edge and trailing edge together with a limit for the maximum grid spacing of 0·075 behind the hydrofoil for simulating wave propagation. The grid system is rearranged at each time step to fit the deforming free surface boundary. The computation is started at the initial conditions of zero velocity and pressure everywhere and a flat free surface ($h = 0$), which satisfy all the boundary conditions. An accelerating process is achieved by adding an inertia term in the u-momentum equation of (1) until the 1000th time step, when the upstream velocity becomes uniform. The time increment is 0·001. Coefficients for the fourth-order numerical dissipation term are set to 5·0 for both the ξ- and η-directions.

The computation is carried out until $T = 16{\cdot}1$, when the flow field is thought to be stationary with a residual level of pressure increment of about $1{\cdot}0 \times 10^{-6}$. Figure 4 illustrates the time history variation in the lift and drag coefficients, showing that both of them tend to reach a stable state from $T = 13$. Notice that the stable lift coefficient of around 0·57 shows excellent agreement with the experiment[9] and that the drag coefficient of approximately 0·009 is also in good agreement with the experiment.[9] The wave profile is compared with the measurement[2] and the results[3] by the MAC method in Figure 5. The present method shows much improvement in wave calculation compared with the MAC method, presumably owing to the use of the free-surface-fitted grid system and the implicit scheme for the free surface elevation solution.

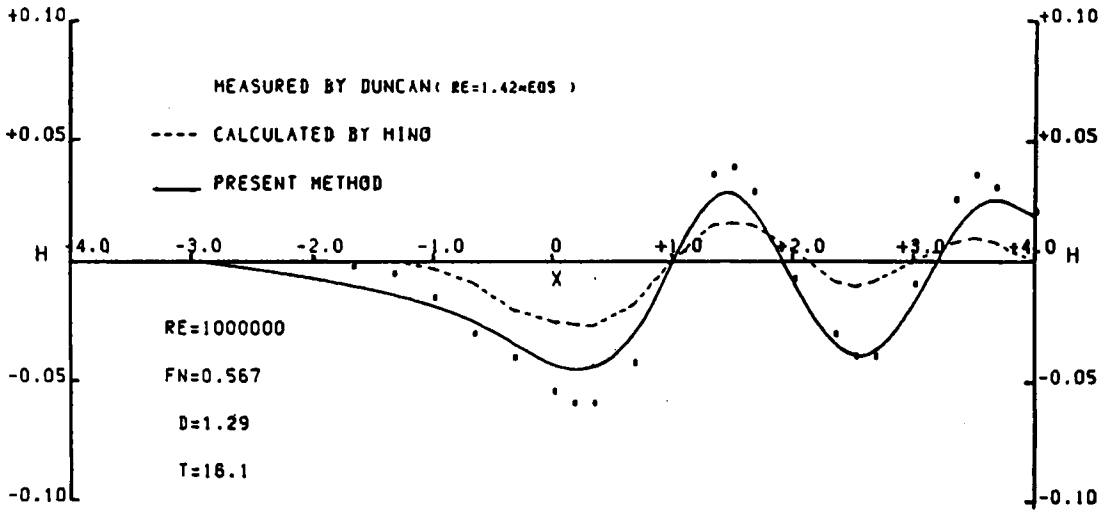

Figure 5. Comparison of wave profiles (2D)

From a close-up view of the velocity vectors around the hydrofoil in Figure 6(a), no separation is detected near the trailing edge because of the introduction of the turbulence model. The pressure distributions on the face and back of the wing section are shown in Figure 6(b), in which a reasonable negative pressure peak on the back near the leading edge is obtained.

4.2. Three-dimensional problem

The wave and turbulent flow past a thin Wigley ship model whose hull form is given by the formula below, at a Reynolds number $Re = 1{\cdot}0 \times 10^6$ and a Froude number $Fn = 0{\cdot}25$, is computed with the three-dimensional code.

Wigley ship model. The equation of the hull form is

$$y = \frac{B}{2}\left[1 - \left(\frac{2x}{L}\right)^2\right]\left[1 - \left(\frac{z}{D}\right)^2\right],$$

where the length $L = 1{\cdot}0$, the breadth $B = 0{\cdot}1$ and the draft $D = 0{\cdot}0625$. An H–O-type grid topology as shown in Figure 7 (at $T = 3{\cdot}0$), with a region of $x(-0{\cdot}7, 1{\cdot}0)$, $y(0{\cdot}0, 0{\cdot}4)$, $z(-0{\cdot}2, 0{\cdot}0)$ and grids of $75 \times 25 \times 17$, is used. The grids are clustered to the solid wall with a minimum grid spacing of 0·001 adjacent to the wall and the symmetrical plane in the η-direction, and to the free surface with a minimum grid spacing of 0·002 in the ζ-direction. In the ξ-direction the grids are distributed densely near the fore part and stern with a maximum grid spacing of 0·055 for simulating wave propagation. The grid system is rearranged at each time step to fit the deforming free surface boundary. The grid points of the intersection between the free surface and solid wall are set to be able to move freely along the hull surface. The computation is started at the initial conditions of zero velocity and pressure everywhere and a flat free surface ($h = 0$), which satisfy all the boundary conditions. An acceleration process is achieved by adding an inertia term in the u-momentum equation of (1) until the 1000th time step, when the upstream

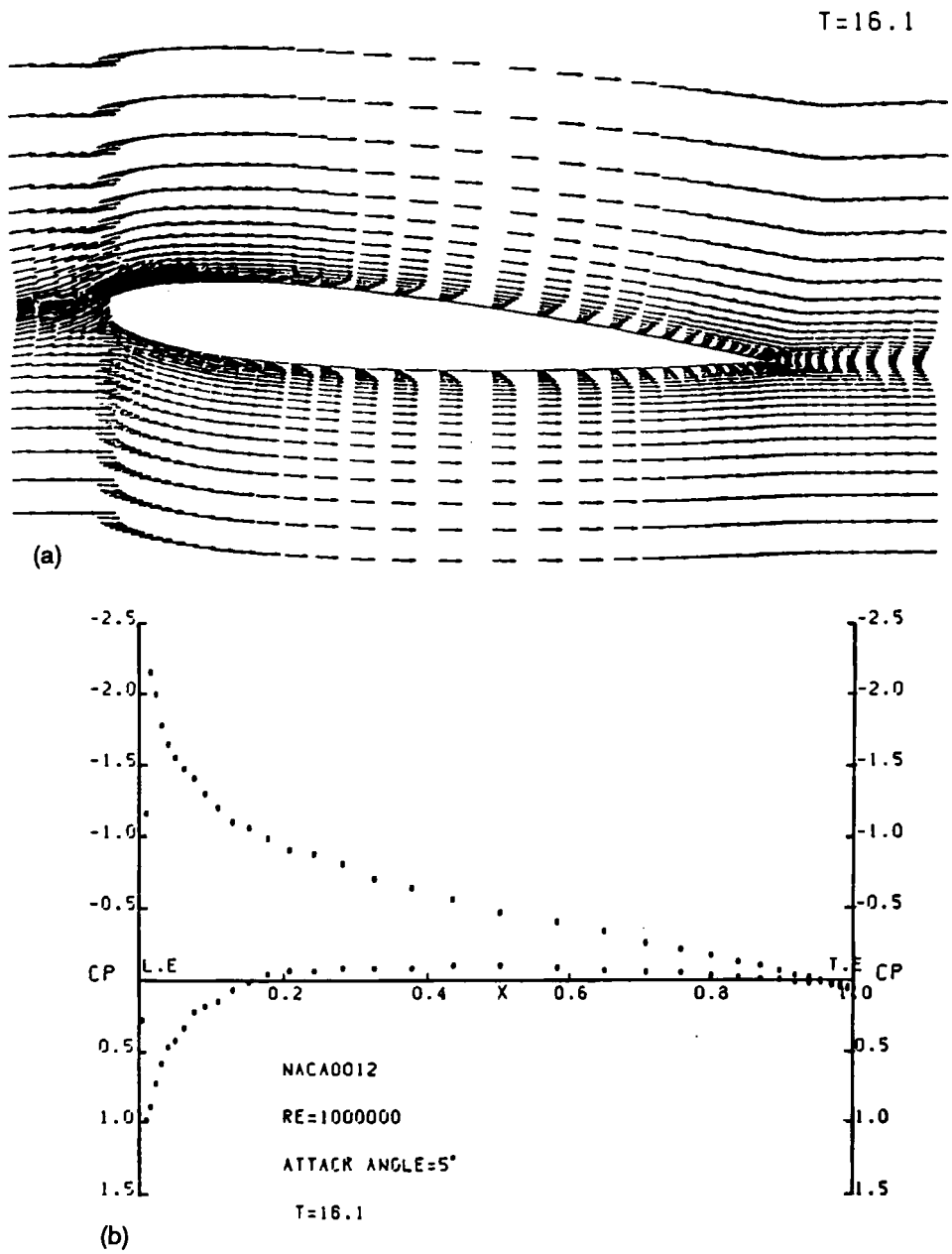

Figure 6. (a) Velocity profiles and (b) pressure distribution (2D)

velocity becomes uniform. The time increment is 0·001 and the coefficients of numerical dissipation terms are set to 5·0.

The computation is performed until $T = 3{\cdot}0$, when the flow field is thought to become steady state with a residual level of pressure increment of about $1{\cdot}0 \times 10^{-6}$. Notice that from the velocity vectors of six sections in the y–z plane illustrated in Figure 8, large cross-flows not only near the bow but also around the stern and in the wake are detected. Furthermore, a longitudinal

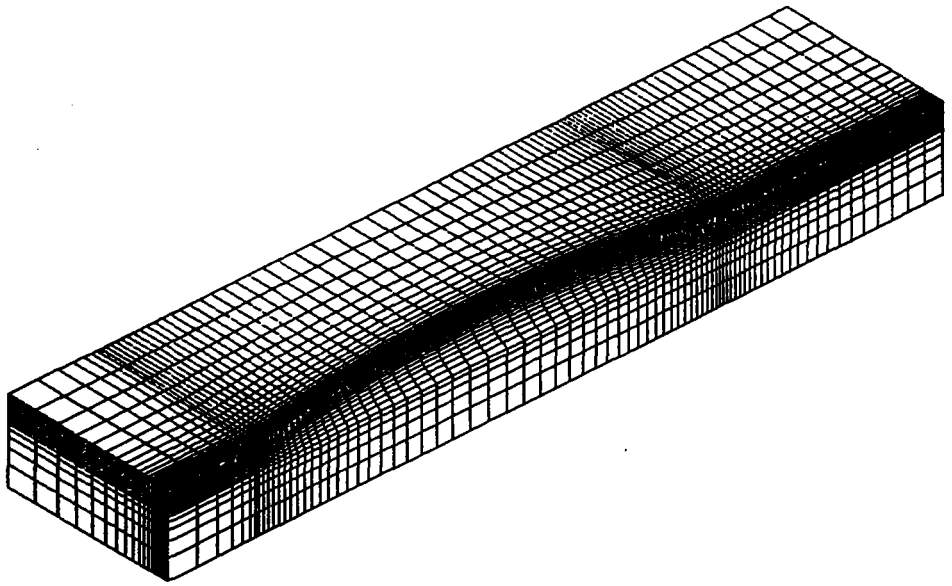

Figure 7. Grid system around Wigley model

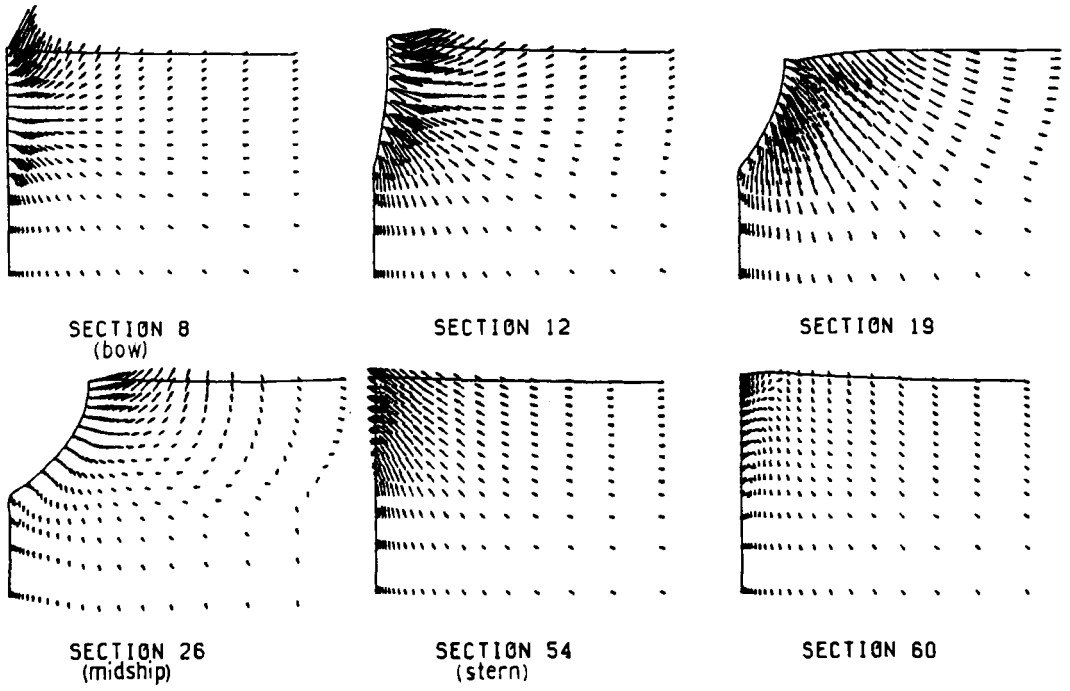

Figure 8. Velocity vectors at various sections

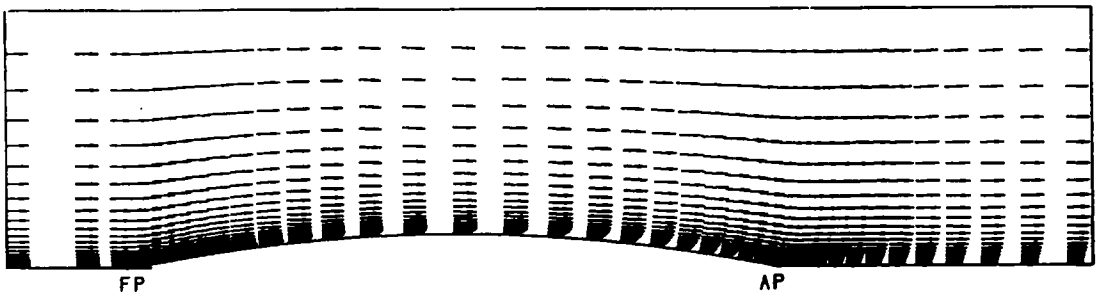

Figure 9. Velocity profiles on free surface

vortex can be found in the wake as shown at section 60, which is believed to be due to the pressure difference between the keel-line and the water-line. Figure 9 shows the velocity profile on the free surface. The thickness of the boundary layer becomes less near the stern and in the wake in comparison with that of the laminar calculation. This phenomenon appears to be due to the interaction between the turbulent boundary and free surface waves. With the implementation of the turbulence model the wave profile along the hull side of ship model shows good agreement with the measurement in Figure 10, since the unexpected wave damping due to the laminar boundary does not occur. The wave pattern in Figure 11 and the iso-wave contours in Figure 12 at $T = 3{\cdot}0$, indicate that the prominent transverse and diverging waves are also well simulated. Equi-pressure contours on the hull surface are shown in Figure 13 and shear stress vectors are evaluated as illustrated in Figure 14. A reasonable pressure distribution can be seen, since the free surface elevation dominates the pressure near the free surface and this also strongly influences the pressure on the hull surface. Resistance coefficients consisting of the pressure resistance coefficient and the frictional resistance coefficient, given in Table I, are computed by integrating the pressures and shear stresses over the whole hull surface. By comparison between the measurements and computed results, it seems that the pressure resistance coefficient shows

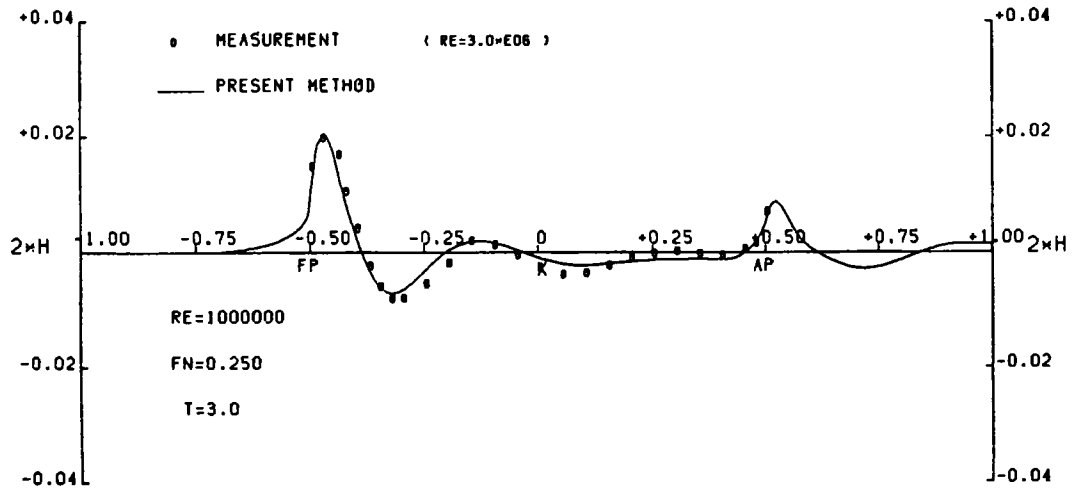

Figure 10. Wave configuration

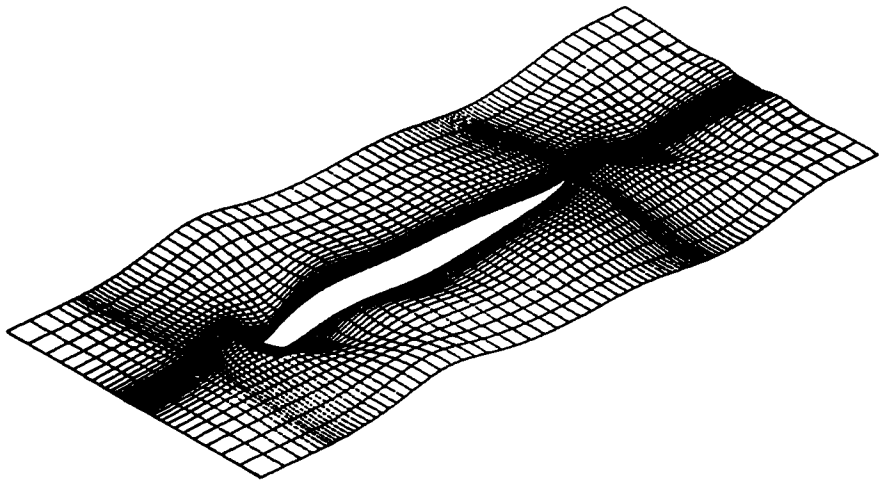

Figure 11. Computed wave pattern

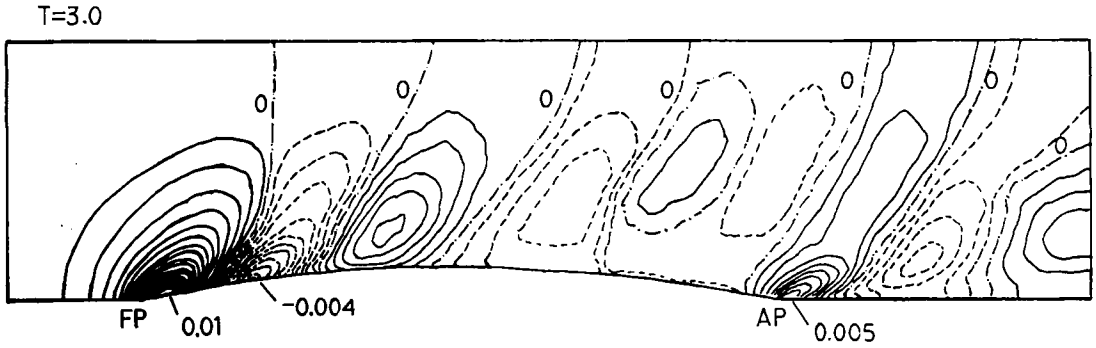

Figure 12. Computed wave contours

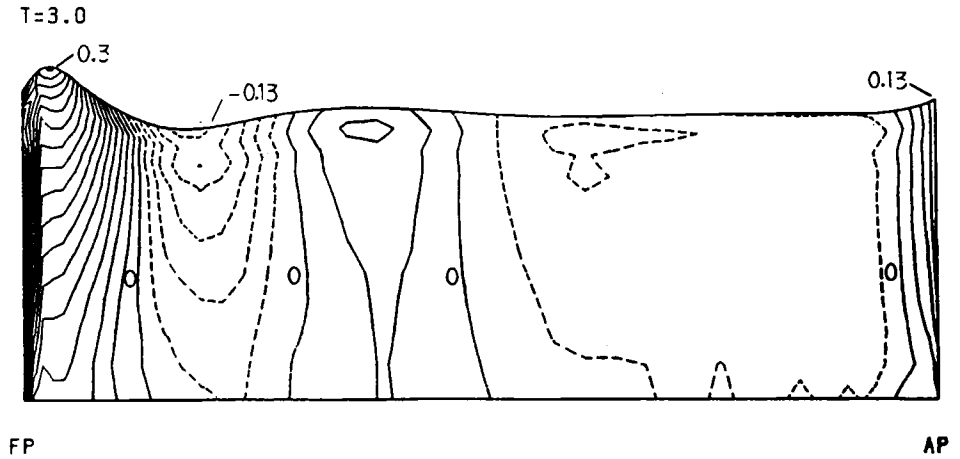

Figure 13. Computed equi-pressure contours on hull surface

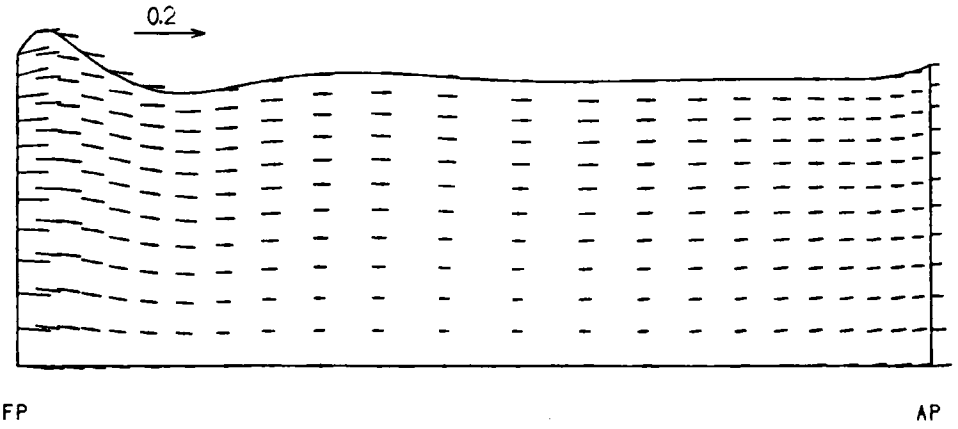

Figure 14. Shear stress distribution on hull surface

Table I. Comparison of resistance coefficients (3D)

	C_p	C_f	C_t
Experiment, $Re = 1{\cdot}2 \times 10^6$	$1{\cdot}010 \times 10^{-3}$	$2{\cdot}808 \times 10^{-3}$	$3{\cdot}818 \times 10^{-3}$
Present method, $Re = 10^6$	$1{\cdot}003 \times 10^{-3}$	$2{\cdot}401 \times 10^{-3}$	$3{\cdot}401 \times 10^{-3}$

good agreement but the frictional coefficient does not. The frictional resistance coefficient of the turbulent calculation shows a lower value than that given by the flat plate formula. This is thought to be because the minimum grid spacing near the hull surface in the spanwise direction is not sufficiently small. The effects of further grid resolution on the improvement of the resistance calculation should be investigated. Also, perhaps the introduction of a wall function would show improvement in the case of relatively coarse grids.

4.3. Validation analysis and discussion

In the present study the following convergence criterion is used:

$$\frac{\sqrt{(\Delta u_{\max}^2 + \Delta v_{\max}^2 + \Delta w_{\max}^2)}}{\sqrt{(U_0^2 + V_0^2 + W_0^2)}} < \varepsilon, \quad \Delta\phi_{\max} < \varepsilon, \quad \Delta h_{\max} < \varepsilon, \tag{26}$$

where ε is set equal to 10^{-6}.

Throughout the present calculation it is understood that the grid system plays an important role in computing the viscous flow, especially the free surface flow, since the maximum spacing and the number of grids inside one wavelength affect the accuracy of the solution and even whether a wave can propagate reasonably or not. Since the implicit scheme is adopted for the calculation of wave height as well as of velocity and pressure, a large grid spacing is expected to be employed in order to save computing time, but it seems that the free surface calculation makes more crucial demands on grid division than velocity and pressure. In addition, it can be stated that the orthogonality of grids and the clustering inside the boundary layer are quite important in estimating the velocity profile and pressure distribution. The orthogonal grid lines

near the wall seem to be able to eliminate the errors in the turbulence calculation. If the number of grids inside the boundary layer is not sufficient, the computed boundary layer will become thicker and strong damping of the stern wave will occur; on the other hand, a large number of grids will lead to a longer computing time, especially in the three-dimensional case.

The free surface conditions for pressure and velocity are treated in a simple manner in the present calculation because of the high Reynolds number. We attempted once to employ the stress conditions in setting the boundary conditions for velocity on the free surface of the two-dimensional problem, but no significant change could be found in comparison with the present approach. On the other hand, on the free surface the turbulence is treated the same as on the wall, which means that no free surface effect, which should exist, is considered. The investigation and explanation of the interactive influence between the turbulence and the free surface, i.e. how to derive a correct turbulence model with the free surface effect and how to take into account the turbulence influence on the stress condition on the free surface, are very important and are tasks for the future.

5. CONCLUDING REMARKS

An implicit approximate factorization method for the full Navier–Stokes solution with the pseudocompressibility approach in a moving grid system is developed in simulating the free surface waves around an arbitrary body. By introducing the pseudocompressibility, the governing equations for velocity, i.e. the Navier–Stokes equations, the modified continuity equation for pressure and the equation of the kinematic condition governing the free surface configuration are discretized by the same algorithm and simultaneously marched out in time until a steady state solution is obtained. Since partial differential equations of the same hyperbolic type are given for all the variables such as velocity components, pressure and even free surface configuration, the governing equations are formulated and solved in vector form, which provides convenience in the numerical calculation. With the discretization of the Euler implicit differencing for time derivatives and the five-point differencing for spatial derivatives, a block pentadiagonal linear system can be obtained which is solved by an effective pentadiagonal system solver.

A grid generation method based on beam-bending theory which uses a cubic spline fitting technique is developed, by which the grid system is generated fitting both the body surface and free surface, so as to deal with the free surface boundary conditions easily.

The present method is first used in solving the two-dimensional free surface viscous flow around a submerged hydrofoil at $Re = 1{\cdot}0 \times 10^6$. Comparison with measurements shows that the present method can predict two-dimensional free surface viscous flow reasonably well.

The method is then employed in solving the three-dimensional free surface viscous flow past a ship model at $Re = 1{\cdot}0 \times 10^6$. Although the wave profiles and pressures show reasonable results in comparison with the experimental results, there remain some points which have to be investigated further, such as the grid resolution for the resistance calculation and the interaction between turbulence and the free surface.

ACKNOWLEDGEMENTS

We would like to acknowledge Assistant Professor K. Suzuki for his significant comments. We extend our thanks to H. Yamasaki, I. Okata and all the Fluid Mechanics staff in the Department of Naval Architecture and Ocean Engineering at Yokohama National University for their support. This work was partially supported by a Grant-in-Aid for Cooperative Research by the

Ministry of Education, Science and Culture and was performed using the computer centres of Tokyo University and Yokohama National University.

APPENDIX: NOMENCLATURE

x, y, z	Cartesian co-ordinate system
ξ, η, ζ	curvilinear co-ordinate system
x_t, y_t, z_t	grid velocity components
u, v, w	Cartesian velocity components
p	pressure
p_a	atmospheric pressure
ϕ	pressure in which hydrostatic pressure is excluded
U, V, W	contravariant velocity components
Re	Reynolds number
Fn	Froude number
ν	eddy viscosity
h	free surface elevation
$()_{i,j}$	partial derivatives
C_p	pressure resistance coefficient: $C_p = P/\frac{1}{2}\rho U_0^2 S$, where ρ is density, U_0 is freestream speed and S is surface area
C_f	frictional resistance coefficient: $C_f = F/\frac{1}{2}\rho U_0^2 S$
C_t	total resistance coefficient: $C_t = C_p + C_f$

REFERENCES

1. F. H. Harlow and J. E. Welch, 'Numerical calculation of time-dependent viscous incompressible flow of fluid with free surface', *Phys. Fluids*, **8**, (1964).
2. R. M. Coleman, 'Nonlinear calculation of breaking and non-breaking waves behind a two-dimensional hydrofoil', *Proc. 16th Symp. on Naval Hydrodynamics*, 1986.
3. T. Hino, 'Numerical computation of a free surface flow around a submerged hydrofoil by the Euler/Navier–Stokes equations', *J. Soc. Naval Archit. Jpn.*, **164**, (1988).
4. J. F. Thompson, F. C. Themes and C. W. Mastin, 'Automatic numerical generation of body-fitted curvilinear coordinate system for fields containing number of arbitrary two-dimensional bodies', *J. Comput. Phys.*, **15**, (1974).
5. A. J. Chorin, *J. Comput. Phys.*, **2**, (1967).
6. Y. Kodana, 'Computation of high Reynolds number flows past a ship hull using the IAF scheme', *J. Soc. Naval Archit. Jpn.*, **161**, (1987).
7. W. M. Chan and J. L. Steger, *AIAA Paper 91-1588-CP*, 1991.
8. P. Bradshaw, T. Cebeci and J. H. Whitelaw, *Engineering Calculation Methods for Turbulent Flow*, Academic, New York, 1981.
9. I. H. Abbott and I. H. Doenhoff, *Theory of Wing Sections*, Dover, New York, 1957.
10. 'Cooperative experiments on Wigley parabolic models in Japan', *17th ITTC Resistance Committee Rep.*, 1983.